

# A Statistical Study of CME Properties and of the Correlation Between Flares and CMEs over Solar Cycles 23 and 24

A. Compagnino<sup>1</sup>  · P. Romano<sup>2</sup> · F. Zuccarello<sup>1</sup>

Received: 11 April 2016 / Accepted: 23 November 2016 / Published online: 7 December 2016  
© Springer Science+Business Media Dordrecht 2016

**Abstract** We investigated some properties of coronal mass ejections (CMEs), such as speed, acceleration, polar angle, angular width, and mass, using data acquired by the *Large Angle Spectrometric Coronagraph* (LASCO) onboard the *Solar and Heliospheric Observatory* (SOHO) from 31 July 1997 to 31 March 2014, *i.e.* during the Solar Cycles 23 and 24. We used two CME catalogs: one provided by the *Coordinated Data Analysis Workshops* (CDAW) Data Center and one obtained by the *Computer Aided CME Tracking software* (CACTus) detection algorithm. For each dataset, we found that the number of CMEs observed during the peak of Cycle 24 was higher than or comparable to the number during Cycle 23, although the photospheric activity during Cycle 24 was weaker than during Cycle 23. Using the CMEs detected by CACTus, we noted that the number of events [ $N$ ] is of the same order of magnitude during the peaks of the two cycles, but the peak of the CME distribution during Cycle 24 is more extended in time ( $N > 1500$  during 2012 and 2013). We ascribe the discrepancy between the CDAW and CACTus results to the observer bias for CME definition in the CDAW catalog. We also used a dataset containing 19,811 flares of C-, M-, and X-class observed by the *Geostationary Operational Environmental Satellite* (GOES) during the same period. Using both datasets, we studied the relationship between the mass ejected by the CMEs and the flux emitted during the corresponding flares: we found 11,441 flares that were temporally correlated with CMEs for CDAW and 9120 for CACTus. Moreover, we found a log–linear relationship between the flux of the flares integrated from the start to end in the 0.1–0.8 nm range and the CME mass. We also found some differences in the mean CMEs velocity and acceleration between the events associated with flares and those that were not.

**Keywords** Coronal mass ejections · Initiation and propagation · Flares · Dynamics

---

✉ A. Compagnino  
[acomp@oact.inaf.it](mailto:acomp@oact.inaf.it)

<sup>1</sup> Dipartimento di Fisica e Astronomia, Università di Catania, Via S. Sofia 78, 95123, Catania, Italy

<sup>2</sup> INAF, Osservatorio Astrofisico di Catania, Via S. Sofia 78, 95123, Catania, Italy

## 1. Introduction

Many studies of eruptive phenomena occurring in the solar atmosphere, such as flares, filament eruptions, and coronal mass ejections (CMEs), are aimed at understanding the role that the global and local magnetic fields play in triggering these phenomena. According to the most recent theoretical and observational works, flares, filaments, and CMEs are all manifestations of the same physical phenomenon: magnetic reconnection. However, the temporal and spatial relationships among these events are still unclear. A preliminary aspect in this type of investigation concerns the properties of CMEs.

For instance, Ivanov and Obridko (2001) studied the semiannual mean CME velocities for the time interval 1979–1989 and revealed a complex cyclic variation with a peak at the solar-cycle maximum and a secondary peak at the minimum of the cycle. The growth of the mean CME velocity is accompanied by a growth of the mean CME width. Moreover, the authors concluded that the secondary peak of the semiannual mean CME velocity in 1985–1986 is due to a significant contribution of fast CMEs with a width of about  $100^\circ$  at the minimum of the cycle. This peak is assumed to be due to the increasing role of the global large-scale magnetic-field system at the minimum of the solar cycle.

Chen, Chen, and Fang (2006) reexamined whether flare-associated CMEs and filament-eruption-associated CMEs have distinct velocity distributions and investigated which factors may affect the CME velocities. They divided the CME events observed from 2001–2003 into three types: the flare-associated type, the filament-eruption-associated type, and the intermediate type. For the filament-eruption-associated CMEs, the speeds were found to be strongly correlated with the average magnetic field in the filament channel.

Cremades and St. Cyr (2007) presented a survey of events observed during the period 1980–2005 and found that the latitude of a CME matches the location of coronal streamers well, in agreement with Hundhausen (1993).

More recently, Mittal *et al.* (2009) have analyzed more than 12,900 CMEs observed by the *Solar and Heliospheric Observatory* (SOHO)/*Large Angle Spectrometric Coronagraph* (LASCO) during the period 1996–2007. They found that the speeds decrease in the decay phase of Solar Cycle 23. There is an unusual drop in speed in 2001 and an abnormal increase in speed in 2003. This increase corresponded to the so-called Halloween events, *i.e.* the high concentration of CMEs, X-class flares, solar energetic particle (SEP) events, and interplanetary shocks that were observed during October and November of that year. The same dataset showed that about 66 % of CMEs have negative acceleration, 25 % have positive acceleration, and the remaining 9 % have very low acceleration (Mittal and Narain, 2009) in the outer corona.

Some difficulties in understanding the relationships between flares and CMEs are due to the different methods of observation that must be used to investigate these phenomena. The coronagraphs that are used to observe the outer corona where the CMEs are detected occult the solar disk and do not allow observing the source region where the corresponding flares take place. Therefore, many authors have tried to study these relationships from a statistical point of view.

For example, St. Cyr and Webb (1991) considered a dataset of two years, *i.e.* from 1984 to 1986 acquired by the *Solar Maximum Mission* (SMM: Phillips, 1990) (see Table 1), and found that 76 % of the CMEs were associated with erupting prominences, 26 % with H $\alpha$  flares, and 74 % with flares observed in the X-ray range. Gilbert *et al.* (2000) analyzed 18 CMEs observed by LASCO-C2 (Brueckner *et al.*, 1995) and the ground-based *Mark-III K-Coronameter* (MK3) at the *Mauna Loa Solar Observatory* (MLSO: MacQueen and Fisher, 1983; St. Cyr *et al.*, 1999) and 54 flares observed in H $\alpha$  during two years of obser-

**Table 1** Previous results on the correlation between CMEs, flares, and eruptive prominences.

| Authors                      | Number of events | Period    | CMEs associated with eruptive prominences | CMEs associated with H $\alpha$ flares | CMEs associated with X-ray flares |
|------------------------------|------------------|-----------|---|--|-----------------------------------|
| St. Cyr and Webb (1991)      | 73 CMEs          | 1984–1986 | 76 %                                      | 26 %                                   | 74 %                              |
| Gilbert <i>et al.</i> (2000) | 18 CMEs          | 1996–1998 | 76 %                                      | 94 %                                   |                                   |
| Subramanian and Dere (2001)  | 32 CMEs          | 1996–1998 | 59 %                                      |  |                                   |
| Zhou, Wang, and Cao (2003)   | 197 CMEs         | 1997–2001 | 94 %                                      | 88 %                                   |                                   |

variation, between 1996 and 1998, and found that 94 % of the H $\alpha$  flares were associated with CMEs, and that 76 % of the CMEs were associated with eruptive prominences. Moreover, analyzing the same period, Subramanian and Dere (2001) used LASCO and the *Extreme Ultraviolet Imaging Telescope* (EIT) instrument Soho, (Delaboudinière *et al.*, 1995) and found that 44 % of the CMEs were associated with eruptions of prominences that were embedded in an active region, while 15 % of those with eruptions occurred outside active regions.

Zhou, Wang, and Cao (2003) used data taken by LASCO onboard SOHO from 1997 to 2001 and selected 197 front-side halo CMEs. They found that 88 % of these CMEs were associated with flares, while 94 % were associated with eruptive filaments. For 59 % of the CMEs, their initiation seemed to precede the associated flare onset recorded by GOES (Howard, 1974; Ludwig and Johnson, 1981), while 41 % of the CMEs seemed to follow the flare onset.

Many authors (see, for example, Gopalswamy *et al.*, 2015a; Gopalswamy *et al.*, 2015b; Youssef, 2012) investigated possible relationships between the CMEs physical parameters and the flare properties, including the narrow CMEs and using only the *Coordinated Data Analysis Workshops* (CDAW) dataset, even though the CACTus catalog was developed around 2004. The authors point out that the list is necessarily incomplete because of the nature of identification. In the absence of a perfect automatic CME-detection program, manual identification is still the best way to identify CMEs (Youssef, 2012).

Using the LASCO and EIT data taken by the SOHO spacecraft, Zhang *et al.* (2001) analyzed four events and found that the impulsive acceleration phase of the selected CMEs coincided well with the rise phase of the associated X-ray flares. Later, Qiu and Yurchyshyn (2005) studied 11 events with varying magnetic-field configurations in the source regions and concluded that the CME velocities were proportional to the total magnetic-reconnection flux, while their kinetic energy was probably independent of the magnetic configuration of the source regions.

An in-depth analysis of the correlation between X-ray flares and CMEs using GOES and LASCO archives from 1996 to 2006 has been performed by Aarnio *et al.* (2011). They considered 13,682 CMEs and selected 826 flare–CME pairs. They found that the CME mass increases with the flare flux, following an approximately log–log relationship:  $\log(\text{CME mass}) = 0.70 \times \log(\text{flare flux})$ , while the CME mass appears unrelated to their acceleration. Aarnio *et al.* (2011) also noted that CMEs associated with flares have higher average linear speeds ( $495 \pm 8 \text{ km s}^{-1}$ ) and negative average acceleration ( $-1.8 \pm 0.1 \text{ m s}^{-2}$ ), while CMEs not associated with flares have a lower average linear speed ( $422 \pm 3 \text{ km s}^{-1}$ ) and marginally positive average acceleration ( $0.07 \pm 0.25 \text{ m s}^{-2}$ ). Finally, the width of CMEs

was found to be directly correlated with the flare flux: X-class flares are associated with the widest CMEs ( $80^\circ \pm 10^\circ$ ), while B-class flares are associated with the narrowest CMEs ( $42^\circ \pm 1.4^\circ$ ).

In this context, we intend to provide a further contribution to the knowledge of CMEs properties and of the correlation between flares and CMEs. In this article we present results obtained from the analysis of a dataset that is more extended than that of Aarnio *et al.* (2011), including 22,876 CMEs and 19,811 flares of GOES class C, M, and X observed from 31 July 1996 to 31 March 2014. We investigate how some of the previously mentioned relationships vary with the solar cycle. In the next section we describe our dataset, in Section 3 we show our results, and in Section 4 we discuss the results and draw our conclusions.

## 2. Data Description

The CMEs data used in this work were acquired by the LASCO-C2 and -C3 coronagraphs onboard SOHO in about 17 years (from 31 July 1997 to 31 March 2014). We used the CDAW Data Center online CME catalog, which is available at the following link: [cdaw.gsfc.nasa.gov/CME\\_list](http://cdaw.gsfc.nasa.gov/CME_list), and the catalog obtained by the *Computer Aided CME Tracking software* (CACTus), which is available at the following link: [sidc.oma.be/cactus/](http://sidc.oma.be/cactus/). These two catalogs allowed us to compare the results from manual identification of CMEs (CDAW) and automatic tracking of CMEs (CACTus). The CDAW catalog contains information on several CME parameters, such as their central polar angle (PA), *i.e.* the mean angle between the two outer edges of the CME width measured counterclockwise from Solar North in degrees on the plane of the sky, the linear velocity, the acceleration, the width, the mass, and the energy. The CACTus catalog contains the entire information of the CDAW catalog except for the mass, the energy, and the acceleration of the events. We remark that the CME start time reported in these catalogs corresponds to the first detection of the CME in the LASCO-C2 field of view, *i.e.* the region from 2.0 to 6.0 solar radii. The whole CDAW dataset contains 22,876 events, while CACTus contains 15,515 events. We also considered 19,811 flares of C-, M-, and X-class that occurred during the same time interval and were observed by GOES. We used the reports of the National Geophysical Data Center (NGDC: <ftp://ftp.ngdc.noaa.gov/>) to collect the main information, such as the time of the beginning, maximum, and end of each flare, the GOES X-ray class, and the integrated flux from the beginning to the end. We considered 17,712 C-class flares, *i.e.* 89.40 %, 1884 M-class flares, *i.e.* 9.51 %, and 155 X-class flares, *i.e.* 0.78 %. We also took into account the location on the solar disk where the flares occurred for 10,742 flares (about 50 %), when this information was reported.

## 3. Results

### 3.1. CME Parameters over the Solar Cycles

In order to show the occurrence distribution of CMEs during the solar-activity cycle, we report in Figure 1 the number of CMEs [ $N$ ] observed by LASCO during each year of our observation time interval (the black and the dot-dashed-blue lines correspond to the data obtained from the CDAW and CACTus catalogs, respectively). We clearly see two peaks that correspond to the maxima of Solar Cycles 23 and 24. In particular, we note that for the CDAW dataset the peak of Cycle 24 is higher than the peak in Cycle 23. This result seems

**Figure 1** Number of CMEs per year observed by LASCO during the selected time interval. The black and dot-dashed-blue lines indicate the results for the CDAW and CACTus catalogs, respectively. The long-dashed-red line indicates the yearly Wolf number during the same period.

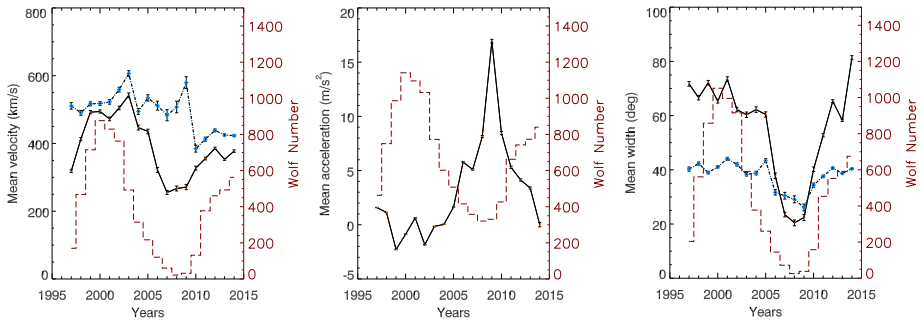
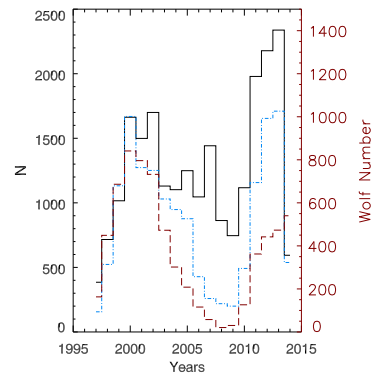


**Figure 2** Distribution of the mean annual CME velocity (left panel), acceleration (middle panel), and angular width (right panel) from 1996 to 2014. The black and dot-dashed-blue lines indicate the results for the CDAW and CACTus catalogs, respectively. In each panel the yearly Wolf number is shown (long-dashed-red line). The blue diamonds indicate the CACTus data.

to be in contrast with the fact that the magnetic activity during Cycle 24 was weaker than during Cycle 23 (Tripathy, Jain, and Hill, 2015), as shown in Figure 1 (long-dashed-red line), where the yearly Wolf number is reported. Moreover, using the CMEs detected by CACTus, we note that  $N$  is on the same order of magnitude during the peaks of the two cycles, and that the peak of the CME distribution during Cycle 24 is more extended in time ( $N > 1500$  during 2012 and 2013). The different results obtained from CDAW and CACTus could be ascribed to the observer bias in the CME definition in the CDAW catalog (Robbrecht, Berghmans, and Van der Linden, 2009; Webb and Howard, 2012; Yashiro, Michalek, and Gopalswamy, 2008). Moreover, in the context of the higher or comparable number of CMEs recorded during Cycle 24, despite the low number of sunspots observed during this cycle, we recall that Gopalswamy *et al.* (2015b) found a similar result from the analysis of halo CMEs.

In Figure 2 (from left to right) we show the behavior of the average annual velocity, acceleration, and angular width for all the observed CMEs during Solar Cycles 23 and 24. For the velocity and the angular width we plot the results of the CDAW dataset (black line) and of the CACTus dataset (dot-dashed-blue line), while for the acceleration we only show the CDAW results because this parameter is not available in the CACTus dataset. The blue diamonds indicate the CACTus data.

We calculated the CME annual mean velocity by considering the total number of CMEs for each year and then considering the velocity averaged with respect to this number. The

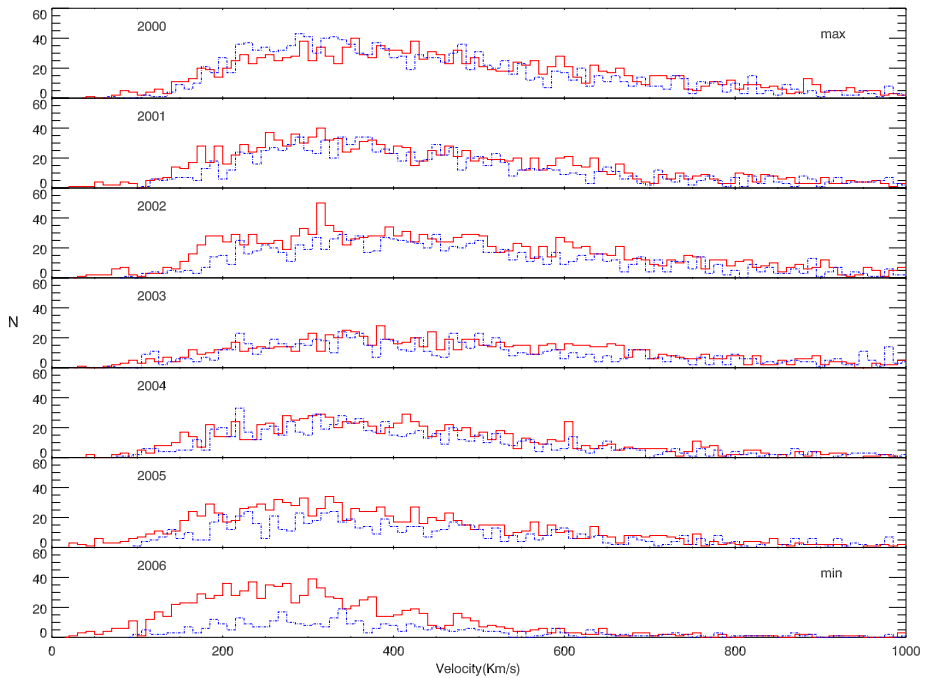


**Figure 3** Distribution of the CME velocity in each year between 2000 and 2006 for the CDAW (red line) and CACTus catalogs (dot-dashed-blue line).

same procedure was applied for the other parameters. We also computed the error bars for the mean distribution of these quantities as  $\sigma/\sqrt{N}$ , where  $\sigma$  is the standard deviation of the corresponding quantity and  $N$  is the number of CMEs that occurred in each year. The error bars are smaller than the symbol sizes, although the error for the acceleration is dominated by the uncertainty of the individual measurements. The red line in each panel shows the yearly Wolf number. For the average velocity, a first peak is observed around 2003 and a second peak between 2012 and 2014 in both datasets. The behavior of the two datasets reflects the solar-activity cycles and can be interpreted according to Qiu and Yurchyshyn (2005) as an effect of the magnetic flux involved in the events during the solar maxima. However, one difference between the two datasets is that in the mean-velocity distribution of the CMEs detected by CACTus there is another peak between 2008 and 2010, during the minimum of the solar cycle. A secondary peak was reported by Ivanov and Obridko (2001) from the analysis of CME velocities for the time interval 1979–1989, which was interpreted by these authors as due to a significant contribution of fast CMEs ( $V > 400 \text{ km s}^{-1}$ ) with a width of  $100^\circ$ .

The mean CME acceleration for CDAW is  $3.17 \pm 0.3 \text{ m s}^{-2}$ . In the distribution of the CME average acceleration (middle panel of Figure 2) we see negative values around the maximum of Solar Cycle 23 and a peculiar peak of about  $15 \pm 2.71 \text{ m s}^{-2}$  in 2009. We note that this peak occurs approximately when we observe the minimum in the annual average velocity distribution for CDAW and the second peak of the velocity distribution for CACTus. However, we argue that statistically the slower CMEs are characterized by higher positive acceleration values.

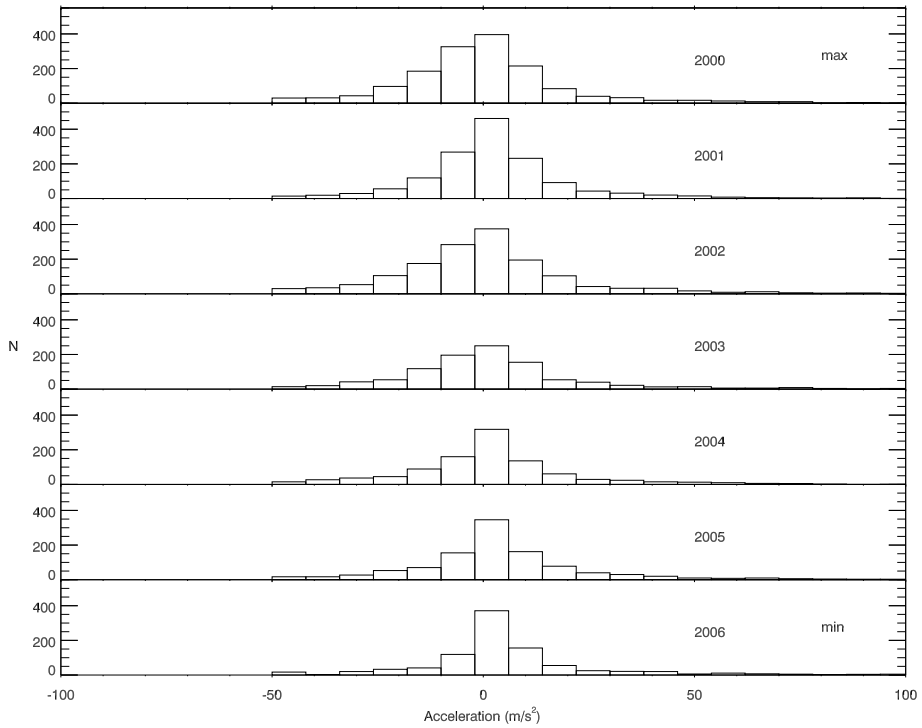


**Figure 4** Distribution of the acceleration of the CMEs in each year between 2000 and 2006.

In Figure 2 (right panel), where we show the mean angular width, the values in 2000–2003 for the CDAW dataset ( $\approx 20^\circ$ ) suggest that on average the narrowest CMEs are the slowest (compare with the left panel of Figure 2) (Yashiro, Michalek, and Gopalswamy, 2008). We also note that for the CACTus dataset the fastest CMEs are the narrowest (Yashiro, Michalek, and Gopalswamy, 2008). Both datasets show a minimum in the mean width distribution over the years that corresponds to the minimum of the solar cycle, although Yashiro, Michalek, and Gopalswamy (2008) found that the CACTus catalog has more narrow CMEs than CDAW. This difference in the two samples determines a different amplitude in the range spanned by the mean angular width distribution, *i.e.* the mean width in the CACTus catalog varies from  $\approx 30^\circ$  during the minimum of solar activity to  $\approx 40^\circ$  during activity maximum, while for the CDAW catalog it varies between  $\approx 20^\circ$  and  $\approx 80^\circ$ .

In order to further analyze the CME properties during the descending part of Solar Cycle 23 (from 2000 to 2006), in Figures 3, 4, and 5 we show the distribution of the velocity, acceleration, and width of the CMEs.

Figure 3 shows that the tail of the velocity distribution decreases from cycle maximum (2000) to minimum (2006). This means that most of the fastest CME velocities ( $> 1000 \text{ km s}^{-1}$ ) occur during the maximum of the solar cycle, when the amount of the magnetic field that emerged in the atmosphere reaches higher values. The average velocity of the CMEs for CDAW during these years is  $396.25 \pm 1.67 \text{ km s}^{-1}$ , where this uncertainty is the standard deviation of the mean, while the mean velocity for CACTus is  $491.78 \pm 2.66 \text{ km s}^{-1}$ . We also remark that Figure 3 shows only a few CMEs that are char-

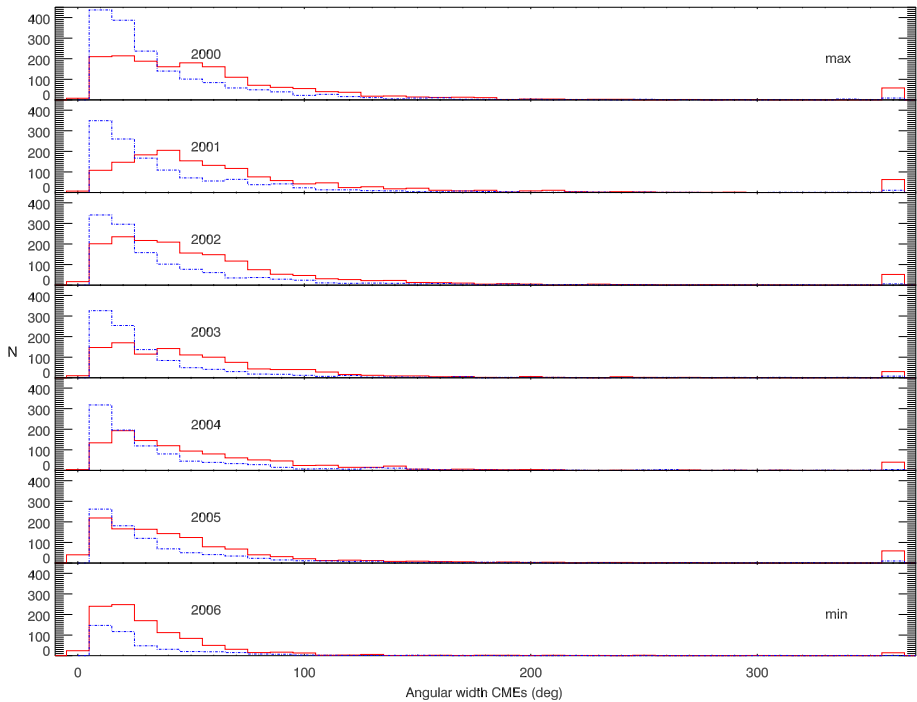


**Figure 5** Distribution of the CME angular width in each year between 2000 and 2006 for CDAW (red line) and CACTus (dot-dashed-blue line). The latter bin refers to halo CMEs.

acterized by velocities  $\geq 600 \text{ km s}^{-1}$  (note that in these plots the velocities are not averaged for each year as in the left panel of Figure 2).

The CME accelerations in each year (Figure 4) are mainly distributed between  $-50 \text{ m s}^{-2}$  and  $50 \text{ m s}^{-2}$ , and few events are characterized by higher values during the solar-cycle maximum. We note an increase in the difference between the negative and positive accelerations while the solar activity decreases. Therefore, the average acceleration per year is mainly negative during the years of higher activity and is positive during the minimum of the solar cycle, as we showed in the middle panel of Figure 2.

The angular-width distribution (see Figure 5) shows that the majority of the CMEs are characterized by an angular width lower than  $100^\circ$ . We note that the CACTus dataset presents a greater number of CMEs narrower than  $40^\circ$  and a smaller number of CMEs wider than  $40^\circ$  than the CDAW dataset (see Yashiro, Michalek, and Gopalswamy, 2008). The mean angular sizes (latitudinal extents) projected against the plane of the sky of all CMEs of the CDAW dataset is  $55.78^\circ \pm 0.44^\circ$ , *i.e.* slightly greater than  $50^\circ$  as found by Cane (2000). The mean CMEs width for the CACTus dataset is  $39.48^\circ \pm 0.38^\circ$ . Only during solar-cycle maximum (2000 and 2001) do we observe a significant number of CMEs with a width larger than  $100^\circ$ . The last bin of the plots in Figure 5 represents the halo CMEs that are contained in the CDAW dataset, *i.e.* CMEs with an angular width of  $360^\circ$ . Our dataset, composed of 22,876 CMEs, contains 616 halo CMEs, *i.e.* 2.69 % of the total number of CMEs.

We used the same sample of years to study the variation in time of the distribution of the polar angle (PA) along which the CME propagated (Figure 6). Both datasets show two peaks centered around the PA that correspond to low latitudes, *i.e.* where the ARs form and



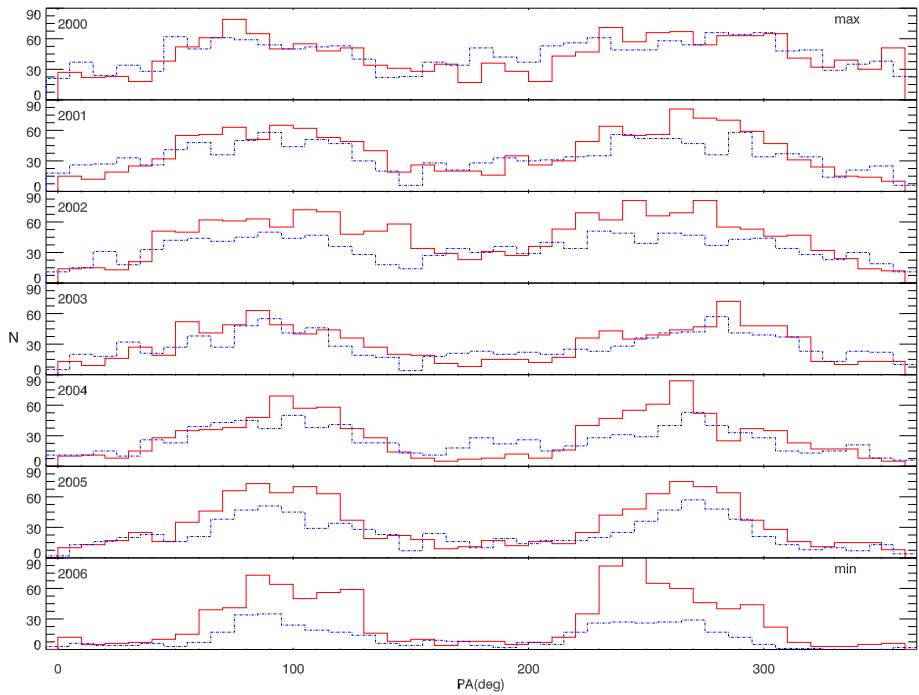


**Figure 6** Distribution of the polar angle (PA) along which the CMEs propagate in each year between 2000 and 2006 for CDAW (red line) and CACTus (dot-dashed-blue line). The PA is measured in degrees from Solar North in counter-clockwise direction.

where the CMEs start. We note that the distribution of PA changes in time from a broader distribution in 2000 (near the maximum of Solar Cycle 23) to a more peaked distribution in 2006 (near solar-activity minimum). We deduce that the latitude distribution of CMEs follows the latitude distribution of the closed-magnetic-field regions in the corona, which is consistent with the fact that the CMEs originate in closed-field regions (Hundhausen, 1993).

### 3.2. Flare Distribution over the Solar Cycles

Using the dataset relevant to flares of C-, M-, and X-class observed by GOES during the period 1996–2014, we determine the total number of flares per year. The result is shown in Figure 7 (black line), which shows two peaks approximately corresponding to the maxima of the solar-activity cycles. The maximum of Solar Cycle 23 is quite long: in 2000, 2001, and 2003, we observed about 2500 flares per year. Furthermore, the flare activity maximum in 2014 corresponds to the peak of the Wolf number in Cycle 24. In 2008 we observed only 11 flares: 10 of C class, and 1 of M class.

When we distinguish among the C-, M-, and X-class flares (Figure 8), we see that the maxima of the M-class flares occurred in 2002 and in 2014, and that both the C- and the M-class flare distribution have a higher maximum during Cycle 23 than during Cycle 24 (we recall that a different result was found for CMEs, see Figure 1).

**Figure 7** Total flare distribution in the selected time interval (black line) and yearly Wolf number (long-dashed-red line).

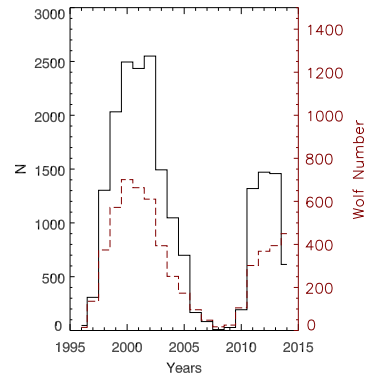
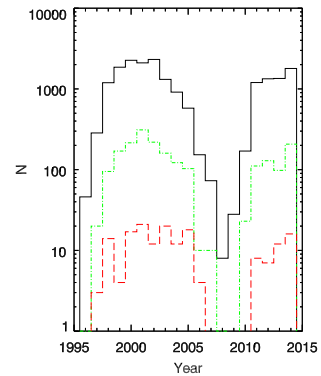


**Figure 8** Distribution of C- (black), M- (dot-dashed-green line), and X-class (long-dashed-red line) flares in the selected time interval.



### 3.3. Correlation Between Flares and CMEs

In order to determine the possible association between one CME and one flare, we used a temporal criterion, requiring that both flare and CME occur within a set time window. We initially set time windows to select the CME first observation time that occurs within  $\pm$  two hours of the flare start time, peak time, or end time, using both datasets. When we consider the CDAW dataset and the flare start time, we find that the highest number of CMEs and flares (59.57 %) is characterized by a difference in time between 10 and 80 minutes (see the black line in the left panel of Figure 9), confirming the results obtained by Aarnio *et al.* (2011). The distribution of the CME-flare-associated events for the CACTus dataset (right panel of Figure 9) is slightly different from the CDAW dataset: We observe a wider time range (from  $-30$  to 110 minutes) for the occurrence of most of the associated events. Considering the flare start time and a time interval of  $\pm$  two hours, we found 11,441 and 9120 flares associated with CMEs using the CDAW and the CACTus catalogs, respectively. The distributions of these flares according to the GOES class are reported in Table 2. In both cases the temporal shift between the flare and the CME decreases if we consider the distributions obtained using the flare-peak time and the flare-end time (see Figure 9). In Tables 2, 3, and 4 we present the associated CMEs-flares using only temporal criteria. In this way, we obtained in first approximation a high number of CMEs associated with flares, which drastically decreases when we apply a spatial correlation between these events to select the true-associated events as described in Section 4, so that finally we found only 1277 CMEs associated with flares that are spatially and temporally correlated.

**Figure 9** Distribution of the CME-flare-associated events as a function of the time difference between the CME first observation and the flare start (black line), peak (dot-dashed-red line), and end time (long-dashed-green line). CT and FT refer to CME first observation time and flare time, respectively. The left and right panels refer to the CDAW and CACTus datasets, respectively.

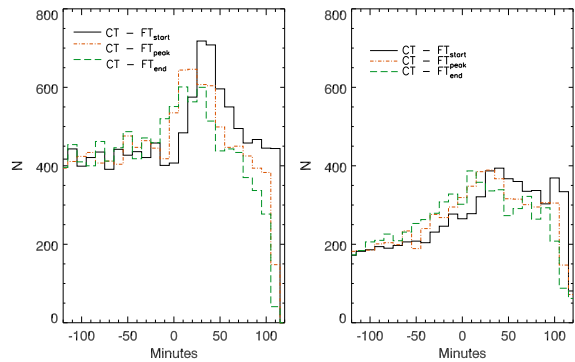


**Table 2** Correlation between CMEs and flares for CDAW and CACTus datasets in the  $\pm$  two hours time interval.

| Flares     |                  | CDAW                                    |                                     | CACTus                                  |                                    |
|------------|------------------|---|-------------------------------------|---|------------------------------------|
| GOES class | Number of events | Flare associated with CME $\pm 2$ h [%] | CMEs not associated with flares [%] | Flare associated with CME $\pm 2$ h [%] | CMEs not associated with flare [%] |
| C          | 17,712           | 10,003 (56.47 %)                        | 11,074 (48.40 %)                    | 7755 (43.78 %)                          | 6396 (41.22 %)                     |
| M          | 1884             | 1308 (69.43 %)                          |                                     | 1242 (65.92 %)                          |                                    |
| X          | 155              | 130 (89.39 %)                           |                                     | 121 (78.06 %)                           |                                    |
| Halo CMEs  | 616              | 315 (51.14 %)                           | 301(48.86 %)                        |   |                                    |

**Table 3** Correlation between CMEs and flares for CDAW and CACTus datasets in the  $\pm$  one-hour time interval.

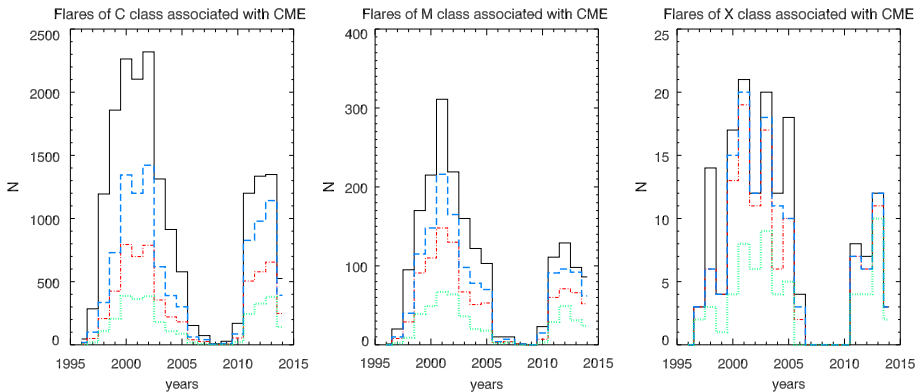
| Flares     |                  | CDAW                                    | CACTus                                  |
|------------|------------------|---|---|
| GOES class | Number of events | Flare associated with CME $\pm 1$ h [%] | Flare associated with CME $\pm 1$ h [%] |
| C          | 17,712           | 5842 (32.98 %)                          | 4228 (23.87 %)                          |
| M          | 1884             | 951 (50.48 %)                           | 771 (40.92 %)                           |
| X          | 155              | 118 (76.13 %)                           | 86 (55.48 %)                            |

The same analysis was performed using the time intervals  $\pm$  one hour,  $\pm 30$  minutes, and the flare start time. The results are reported in Tables 3 and 4. A similar behavior of the correlation between CMEs and flares in different time intervals and in different GOES classes has been found for both datasets. We ascribe the smaller number of CACTus CMEs associated with X-class flares to the limits of the CACTus algorithm in the detection of the fastest CMEs (Yashiro, Michalek, and Gopalswamy, 2008).

The distributions of C-, M-, and X-class flares associated with CMEs, as a function of the year in the solar cycle in the time interval of  $\pm$  two hours,  $\pm$  one hour, and  $\pm 30$  minutes, are shown in Figures 10 and 11 for CDAW and CACTUs, respectively. We note that the probability of finding CMEs associated with flares decreases when the time window is narrower. However, we see that the peak and the shape of the distributions remain similar, independently of the considered temporal time window. In the left panels of Figures 10 and 11,

**Table 4** Correlation between CMEs and flares for CDAW and CACTus datasets in the  $\pm 30$  min time interval.

| Flares     |                  | CDAW                                       | CACTus                                     |
|------------|------------------|--|--|
| GOES class | Number of events | Flare associated with CME $\pm 30$ min [%] | Flare associated with CME $\pm 30$ min [%] |
| C          | 17,712           | 2992 (16.89 %)                             | 2159 (12.19 %)                             |
| M          | 1884             | 445 (23.62 %)                              | 341 (18.099 %)                             |
| X          | 155              | 62 (40.00 %)                               | 37 (23.87 %)                               |

**Figure 10** Total distribution of C-class (left panel), M-class (middle panel), and X-class (right panel) flares associated with the CMEs as a function of years in  $\pm$  two hours time window (long-dashed-blue line), in  $\pm 1$  hour time window (dot-dashed-red line), and  $\pm 30$  minutes time window (dotted-green line) for CDAW. The black line in each panel indicates the distribution of all flares for a given class.

the peaks correspond to 2000–2002 and 2011–2014, in agreement with the solar-activity cycles (see Figure 1). The distribution of C-class flares associated with CMEs (left panels of Figures 10 and 11) shows that these events are also present during the phases of solar-activity minimum. The distribution of M-class flares (middle panels of Figures 10 and 11) shows a trend very similar to the trend found for C-class flares. On the other hand, we note that the distribution of X-class flares associated with CMEs is more uniform across the solar cycle than that of C- and M-class flares for both datasets. For example, for CDAW in 1998 and 2005, we observe 14 and 18 X-class flares associated with CMEs, respectively, while for CACTus we observe 6 and 8 X-class flares in those years, although the magnetic activity was not high. However, when we consider only the flares associated with CMEs in a  $\pm 30$  minute time window, we find a distribution of the X-class flares that is more consistent with the solar cycle for both distributions.

In Figure 12 we show the distribution of the CMEs velocity, distinguishing between events associated with flares in the  $\pm$  two hours time window and events not associated with flares. The mean CMEs velocities in the CDAW datasets for the CMEs associated and not associated with flares are  $472.87 \pm 2.77 \text{ km s}^{-1}$  and  $379.41 \pm 2.25 \text{ km s}^{-1}$ , respectively. The mean CMEs velocities in the CACTus dataset for the CMEs associated and not associated with flares are  $500.62 \pm 3.28 \text{ km s}^{-1}$  and  $437.75 \pm 3.79 \text{ km s}^{-1}$ , respectively. In Figure 12 (right panel) we note that many CMEs are not associated with flares in the CACTus dataset; they have velocities of between 100–200  $\text{km s}^{-1}$ .

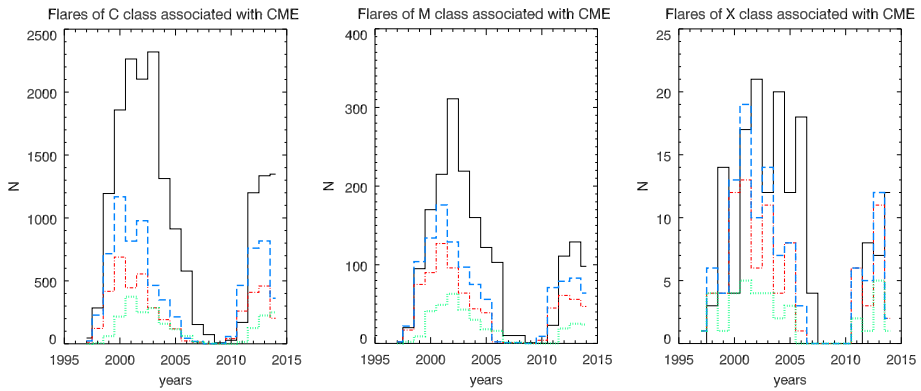
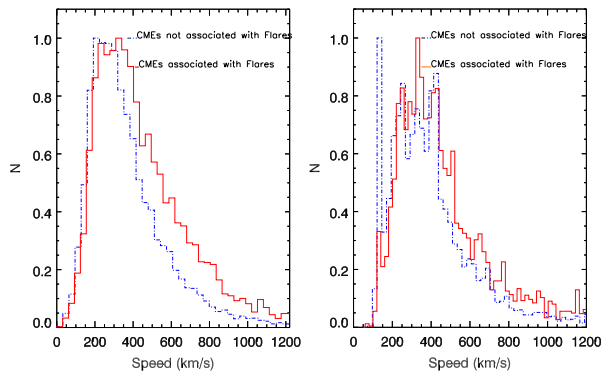


**Figure 11** Total distribution of C-class (left panel), M-class (middle panel), and X-class (right panel) flares associated with the CMEs as a function of years in  $\pm$  two hour time window (long-dashed-blue line), in  $\pm$ 1 hour time window (dot-dashed-red line), and  $\pm$ 30 minute time window (dotted-green line) for CACTus. The black line in each panel indicates the distribution of all flares for a given class.

**Figure 12** Distribution of the CME velocities for the CDAW (left panel) and CACTus (right panel) datasets. The solid red and dot-dashed-blue lines correspond to CMEs associated with flares and not associated with flares, respectively.



The distribution of the CME acceleration (left panel of Figure 13) shows that the CMEs associated with flares have an average acceleration of  $-0.32 \pm 0.34 \text{ m s}^{-2}$ , while the CMEs not associated with flares have an average acceleration of  $3.44 \pm 0.39 \text{ m s}^{-2}$ . In the right panel of Figure 13 we report the distribution of the CME mass. The logarithms of the mean CME mass [g] for CMEs associated with flares and those not associated with flares are  $14.70 \pm 0.006 \text{ g}$  and  $14.54 \pm 0.004$ , respectively.

Furthermore, we found different linear velocity distributions when we distinguish among the three flare classes (Figure 14). The CDAW velocity distribution of the CMEs associated with the C-class flares shows a significant peak at  $250 \text{ km s}^{-1}$  that is absent in the CACTus velocity distribution. For CDAW the mean linear velocities of CMEs associated with flares of C-, M-, and X-classes are  $535.95 \pm 1.11 \text{ km s}^{-1}$ ,  $585.71 \pm 8.16 \text{ km s}^{-1}$ , and  $626.99 \pm 56.58 \text{ km s}^{-1}$ , respectively. For CACTus the mean velocities of CMEs associated with flares of C-, M-, and X-classes are  $487.91 \pm 3.46 \text{ km s}^{-1}$ ,  $562.16 \pm 9.82 \text{ km s}^{-1}$ , and  $688.15 \pm 34.35 \text{ km s}^{-1}$ , respectively.

Both distributions are similar, except that CACTus finds fewer events than CDAW, as we note in the distribution of CMEs associated with C-class flares (see the blue line in Figure 14). It is worth noting that the differences between the velocity of CMEs associated

**Figure 13** Distribution of the CME acceleration (left panel) and mass (right panel) for the CDAW dataset. The solid red and dot-dashed-blue lines correspond to CMEs associated with flares and not associated with flares, respectively.

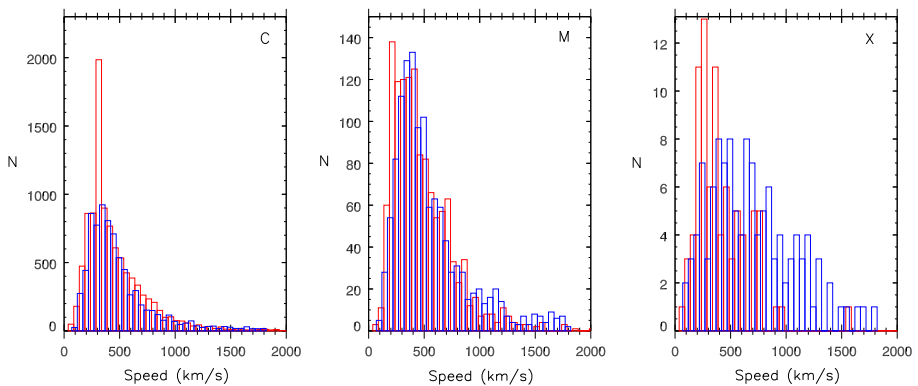
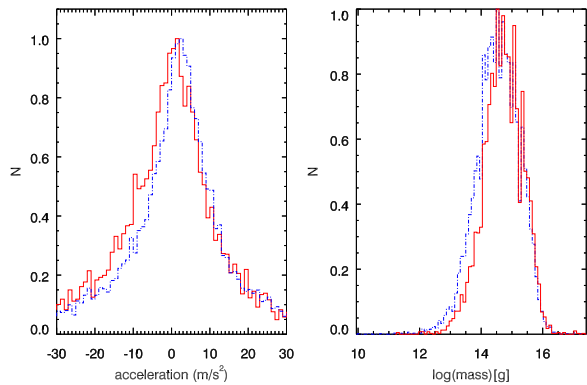


**Figure 14** Distribution of the linear velocity of CMEs associated with flares of C-class (left panel), M-class (middle panel), and X-class (right panel) for CDAW (red line) and CACTus (blue line).

with X-class flares in the CDAW dataset and in the CACTus dataset. The CMEs associated with flares in the CACTus dataset are faster than those of the CDAW dataset.

In Figure 15 we show the relationship between CME speed and acceleration, taking into account the different class of the associated flares. We found that the majority of CMEs that are characterized by higher velocities are associated with accelerations between  $-200$  and  $200 \text{ m s}^{-2}$ . On the other hand, many CMEs have a wide range of accelerations (between  $-400$  and  $400 \text{ m s}^{-2}$ ), but velocities below  $700 \text{ km s}^{-1}$ . These CMEs are mainly associated with C- and M-class flares.

#### 4. CME Parameters and Flare Energy

We used our dataset to investigate the relationship between the logarithm of the flare flux and the logarithm of the CME mass. In this case, we considered not only the temporal correlation between flares and CMEs, but also their spatial correlation. We limited this analysis to flares that occurred in the time window of  $\pm$  two hours and were characterized by a known location of the source region on the solar disk. We associated flares that occurred in the top left quadrant of the solar disk with CMEs characterized by a polar angle between  $0^\circ$  and  $89^\circ$ , flares that occurred in the bottom-left quadrant with CMEs characterized by a polar angle

**Figure 15** Scatter plot of the CME velocity as a function of their acceleration. We distinguish the associated flares of C class (black triangle), M-class (green diamonds), and X class (red square).

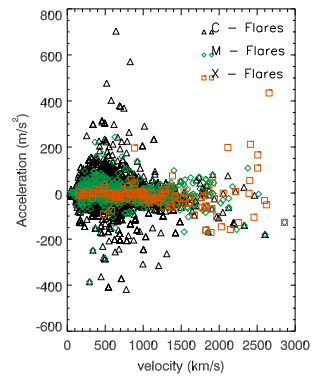
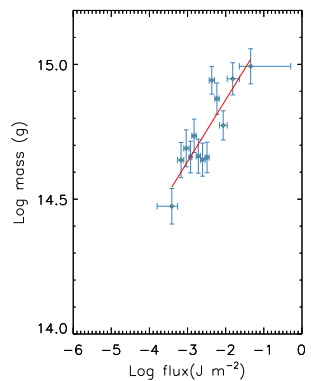


**Figure 16** Relationship between integrated flare flux and CME mass for the CMEs associated with flares in the  $\pm$  two hour time window.



between  $90^\circ$  and  $179^\circ$ , *etc.* This criterion of association between flares and CMEs is based on the assumption that most CMEs propagate nearly radially, according to the standard CME–flare model (see Lin and Forbes, 2000). In this way, we obtained 1277 CMEs that are spatially and temporally correlated with flares. We considered the flux of these flares integrated from their start to end in the 0.1–0.8 nm range. Subsequently, the 1277 CME–flare pairs were binned into 13 equal sets of 100 pairs each, with the exception of the last set, which contains 77 pairs. We computed the mean value of the logarithm of the CME mass and the logarithm of flare flux in each group. The relationship between the logarithm of the CME mass and the logarithm of the flare flux is shown in Figure 16, where we also show the error bars of the logarithm of the CMEs mass computed as  $\sigma/\sqrt{N}$ . The flux error bars correspond to the minimum/maximum flare-flux values spanned by that bin. The results shown in Figure 16 are similar to the result reported by Aarnio *et al.* (2011). We found the following log–linear relationship between integrated flare flux [ $\phi_f$ ] and CME mass [ $m_{CME}$ ]:

$$\log(m_{CME}) = (15.33 \pm 0.10) + (0.23 \pm 0.04) \log(\phi_f). \tag{1}$$

However, it is worth noting that this relationship disappears when we limit the same analysis to each year of our dataset (we do not show the corresponding plots in this article). This means that the log–linear relationship between integrated flare flux and CME mass is only consistent for a large sample of events, but it is not valid during the different phases of the solar cycle.

The unreduced  $\chi^2$ -test of the linear fit that we have performed is 0.07. Further tests to verify the goodness of the fit have also been performed. The Spearman coefficient, indicating how well the relationship between two variables can be described using a monotonic function, is 0.82, which indicates a good correlation between these quantities. We also found a p-value of 0.85 and a linear Pearson correlation coefficient of 0.87.

## 5. Conclusions

In this article we used the huge dataset of CMEs observed for nearly all of the operational time, to date, of the LASCO mission onboard SOHO to infer some properties of these events over Solar Cycles 23 and 24 and to study their correlation with the flares observed in the X-ray range between 1.0 and 8.0 Å by GOES. We used two CME catalogs; one based on manual identification of CMEs (CDAW), and one based on automatic tracking of the CMEs (CACTus).

From our analysis, we conclude that the peak in the number of CMEs in Cycle 24 is higher than the number during Cycle 23. In particular, for the CDAW dataset the number of CMEs at the maximum of Solar Cycle 24 is higher than the number at the maximum of Solar Cycle 23; for CACTus the peaks during the maxima are similar, but the peak corresponding to Solar Cycle 24 is more extended in time than the peak corresponding to Solar Cycle 23. This result seems to be in contrast with the fact that the magnetic activity during Cycle 24 was weaker than during Cycle 23, as noted in the work of Tripathy, Jain, and Hill (2015), who analyzed the frequency shifts of the acoustic solar-mode measurements separately for the two cycles and found that the magnetic activity during Solar Cycle 24 was weaker than during Cycle 23.

Solar Cycle 24 has been extremely weak as measured by the sunspot number (SSN) and is the smallest since the beginning of the space age. The weak activity has been thought to be due to the weak polar field strength in Cycle 23. Several authors have suggested that the decline in Cycle 24 activity might lead to a global minimum (Padmanabhan *et al.*, 2015; Zolotova and Ponyavin, 2014).

From the analysis of the CME average velocity, we found two peaks that reflect the solar-activity cycles and can be interpreted, according to Qiu and Yurchyshyn (2005), as an effect of the magnetic flux involved by the events during the solar maxima, but we also observe another peak at the minimum of the cycles, even if only for the CACTus dataset, in 2009. This peak agrees with the cyclic variation of the CME velocities in the previous solar-activity cycles, as reported by Ivanov and Obridko (2001).

From the distribution of the average acceleration of the CMEs, we see a maximum of about  $15 \text{ ms}^{-2} \pm 2.71 \text{ ms}^{-2}$ , corresponding to the minimum of the distribution of the average velocity (see Figure 2, upper and middle panel). This peak may be due to the contribution of the slower CMEs that occur during solar-activity minimum; these CMEs are characterized by higher positive acceleration values.

We also found that the tail of the higher velocity distribution of the CMEs that were observed during the descending part of Solar Cycle 23 (from 2000 to 2006) is no longer present from the maximum (2000) to the minimum (2006) of the cycle (see Figure 3).

The distribution of the CME angular widths for CDAW shows that on average, the narrower CMEs are slower and the majority of the CMEs are characterized by an angular width lower than  $100^\circ$ . Only during the maximum of the solar cycle (2000 and 2001) do we observe a significant number of CMEs with an angular width larger than  $100 \pm 0.44^\circ$



The CDAW and CACTus datasets present a different amplitude of the range spanned by the mean angular width, *i.e.* for the CACTus catalog the mean width varies from  $\approx 30^\circ$  during solar-activity minimum to  $\approx 40^\circ$  during activity maximum, while for CDAW the mean width varies from  $\approx 20^\circ$  to  $\approx 80^\circ$ .

The latitude distribution of CMEs follows the latitude distribution of the closed magnetic field regions of the corona, which is consistent with the fact that CMEs originate in closed-field regions (Hundhausen, 1993). We also note that the distribution of PA changes in time from a broader distribution in 2000 (near the maximum of Solar Cycle 23) to a more peaked distribution in 2006 (near the minimum of solar activity).

Using the dataset of CMEs and flares, and selecting the event occurring in the same time window of  $\pm$  two hours,  $\pm$  one hour, and  $\pm 30$  minutes, we identified CMEs and flares that are temporally correlated.

Although the number of associated CMEs–flares that are both temporally and spatially correlated might seem low, Aarnio *et al.* (2011), studying the correlation between flare flux and CME mass, found a similar result with 826 associated CMEs–flares during the time interval 1996–2006. Youssef (2012) studied the correlation between flare flux and CME energy, and found 776 associated CME–flares during the time interval 1996–2010. Considering the flare start time, we found that the highest number of CMEs and flares detected in the CDAW dataset (59.57 %) is characterized by a difference in time of between 10 and 80 minutes (see the black line in the left panel of Figure 9), in agreement with Aarnio *et al.* (2011). The CME–flare-associated events for the CACTus dataset show a wider temporal range. We argue that this difference between the two datasets depends on the different criteria used by the observer to define a CME in CDAW. A time window of 10–80 minutes is clear evidence that in many cases the flare occurs before the first observation of the CME in the coronagraph, and taking into account that the temporal resolution of LASCO is about 30 minutes, there are a number of cases in which the flare most likely precedes the CME initiation and may be the first manifestation of the initiation process. We also need to investigate the role of filaments and prominences in the initiation.

The shape of the distributions of C-, M-, and X-class flares associated with CMEs varies with the intensity of the flares (see Figures 10 and 11), but it is similar for both datasets. In particular, we note that the distribution of X-class flares associated with CMEs is quite uniform with respect to the distribution of C- and M-class flares across the solar cycle. However, when we only consider the flares associated with CMEs in the  $\pm 30$  minute time window, we find a distribution of the X-class flares that is more consistent with the solar cycle (see the right panel of Figure 10).

We found that most of the CMEs that are characterized by higher linear velocities are associated with flares (see – *e.g.* – Gosling *et al.* (1976); Moon *et al.* (2003)). The mean velocities for CMEs associated with flares are higher than the velocities for CMEs not associated with flares in both datasets. Our results are therefore very similar to those found by Aarnio *et al.* (2011).

Moreover, our analysis shows that the width of the CMEs associated with flares is positively correlated with the flare flux. The mean angular width of the flares associated with CMEs is  $68.61^\circ$ ,  $116.82^\circ$ , and  $258.49^\circ$  for C-, M-, and X-class flares, respectively.

The distribution of the CME acceleration (left panel of Figure 13) shows that the CMEs associated with flares have an average acceleration of  $-0.32 \pm 0.34 \text{ m s}^{-2}$ , while the CMEs not associated with flares have an average positive acceleration of  $3.44 \pm 0.37 \text{ m s}^{-2}$ . We suggest that these values are slightly different from those found by Aarnio *et al.* (2011) because of the diverse sample of events considered in our article.

We also used our dataset to further extend the study on the log–linear relationship between the flare flux [ $\phi_F$ ] and the CME mass [ $m_{\text{CME}}$ ] performed by Aarnio *et al.* (2011). In

this case, we considered not only the temporal correlation between flares and CMEs, but also their spatial correlation. As mentioned above, this allows us to be more confident that the CMEs and the flares may be linked, although some events may be neglected. We found that  $\log(m_{\text{CME}}) \propto 0.23 \log(\phi_f)$ . The differences between the results of Aarnio *et al.* (2011) and ours may be due to several reasons. First of all, we considered a more extended dataset. We also used the flux of the flares integrated from their start to end in the 0.1–0.8 nm range. Finally, we used different criteria to determine the association between flares and CMEs. Therefore, we conclude that the log–linear relationship is valid not only when we consider the peak of the flare flux, but also when we consider the energy released during the whole event.

It is remarkable that this relationship disappears when we limit the sample of flare–CME pairs to the different phases of the solar cycle. This means that the log–linear relationship is only valid from a statistical point of view, *i.e.* when we consider a large sample of events.

We argue that this result is due to different aspects (intensity of magnetic field, magnetic reconnection, and configuration of sunspots on the solar surface) that influence the evolution of these phenomena. Further study and analysis must be made on the intensity of the magnetic flux that is involved in these phenomena and consequently on the capacity of ejecting the mass into the interplanetary space. The magnetic configuration can play an important role in determining the different ways to build up and release magnetic free energy and the role of magnetic reconnection

**Acknowledgments** The authors wish to thank the anonymous referee for their useful suggestions that allowed us to improve the article. This research work has received funding from the European Commission’s Seventh Framework Programme under the Grant Agreements no. 606862 (F-Chroma project) and no. 312495 (SOLARNET project). This research is also supported by the ITA MIUR-PRIN grant on “The active sun and its effects on space and Earth climate” and by Space WEather Italian COMMunity (SWICO) Research Program. We are also grateful to the University of Catania for providing the Grant FIR 2014.

**Disclosure of Potential Conflicts of Interest** The authors declare that they have no conflicts of interest.

## References

- Aarnio, A.N., Stassun, K.G., Hughes, W.J., McGregor, S.L.: 2011, *Solar Phys.* **268**, 195. [ADS](#). [DOI](#).
- Brueckner, G.E., Howard, R.A., Koomen, M.J., Korendyke, C.M., Michels, D.J., Moses, J.D., Socker, D.G., Dere, K.P., Lamy, P.L., Llebaria, A., Bout, M.V., Schwenn, R., Simnett, G.M., Bedford, D.K., Eyles, C.J.: 1995, *Solar Phys.* **162**, 357. [ADS](#). [DOI](#).
- Cane, H.V.: 2000, *Space Sci. Rev.* **93**, 55. [ADS](#). [DOI](#).
- Chen, A.Q., Chen, P.F., Fang, C.: 2006, *Astron. Astrophys.* **456**, 1153. [ADS](#). [DOI](#).
- Cremades, H., St. Cyr, O.C.: 2007, *Adv. Space Res.* **40**, 1042. [ADS](#). [DOI](#).
- Delaboudinière, J.-P., Artzner, G.E., Brunaud, J., Gabriel, A.H., Hochedez, J.F., Millier, F., Song, X.Y., Au, B., Dere, K.P., Howard, R.A., Kreplin, R., Michels, D.J., Moses, J.D., Defise, J.M., Jamar, C., Rochus, P., Chauvineau, J.P., Marioge, J.P., Catura, R.C., Lemen, J.R., Shing, L., Stern, R.A., Gurman, J.B., Neupert, W.M., Maucherat, A., Clette, F., Cugnon, P., van Dessel, E.L.: 1995, *Solar Phys.* **162**, 291. [ADS](#). [DOI](#).
- Gilbert, H.R., Holzer, T.E., Burkepile, J.T., Hundhausen, A.J.: 2000, *Astrophys. J.* **537**, 503. [ADS](#). [DOI](#).
- Gopalswamy, N., Makela, P., Akiyama, S., Yashiro, S., Thakur, N.: 2015a, *Sun Geosph.* **10**, 111. [arXiv](#). [ADS](#).
- Gopalswamy, N., Xie, H., Akiyama, S., Mäkelä, P., Yashiro, S., Michalek, G.: 2015b, *Astrophys. J. Lett.* **804**, L23. [ADS](#). [DOI](#).
- Gosling, J.T., Hildner, E., MacQueen, R.M., Munro, R.H., Poland, A.I., Ross, C.L.: 1976, *Solar Phys.* **48**, 389. [ADS](#). [DOI](#).
- Howard, M.: 1974, *Spaceflight* **16**, 383. [ADS](#).
- Hundhausen, A.J.: 1993, *J. Geophys. Res.* **98**, 13177. [ADS](#). [DOI](#).
- Ivanov, E.V., Obridko, V.N.: 2001, *Solar Phys.* **198**, 179. [ADS](#). [DOI](#).
- Lin, J., Forbes, T.G.: 2000, *J. Geophys. Res.* **105**, 2375. [ADS](#). [DOI](#).

- Ludwig, G., Johnson, D.: 1981, *Adv. Space Res.* **1**, 23. [ADS](#). [DOI](#).
- MacQueen, R.M., Fisher, R.R.: 1983, *Solar Phys.* **89**, 89. [ADS](#). [DOI](#).
- Mittal, N., Narain, U.: 2009, *New Astron.* **14**, 341. [ADS](#). [DOI](#).
- Mittal, N., Sharma, J., Tomar, V., Narain, U.: 2009, *Planet. Space Sci.* **57**, 53. [ADS](#). [DOI](#).
- Moon, Y.J., Choe, G.S., Wang, H., Park, Y.D., Cheng, C.Z.: 2003, *J. Korean Astron. Soc.* **36**, 61. [ADS](#). [DOI](#).
- Padmanabhan, J., Bisoi, S.K., Ananthakrishnan, S., Tokumaru, M., Fujiki, K., Jose, L., Sridharan, R.: 2015, *J. Geophys. Res.* **120**, 5306. [ADS](#). [DOI](#).
- Phillips, K.: 1990, *Astron. Now* **4**, 28. [ADS](#).
- Qiu, J., Yurchyshyn, V.B.: 2005, *Astrophys. J.* **634**, L121. [ADS](#). [DOI](#).
- Robbrecht, E., Berghmans, D., Van der Linden, R.A.M.: 2009, *Astrophys. J.* **691**, 1222. [ADS](#). [DOI](#).
- St. Cyr, O.C., Webb, D.F.: 1991, *Solar Phys.* **136**, 379. [ADS](#). [DOI](#).
- St. Cyr, O.C., Burkepile, J.T., Hundhausen, A.J., Lecinski, A.R.: 1999, *J. Geophys. Res.* **104**, 12493. [ADS](#). [DOI](#).
- Subramanian, P., Dere, K.P.: 2001, *Astrophys. J.* **561**, 372. [ADS](#). [DOI](#).
- Tripathy, S.C., Jain, K., Hill, F.: 2015, *Astrophys. J.* **812**, 20. [ADS](#). [DOI](#).
- Webb, D.F., Howard, T.A.: 2012, *Living Rev. Solar Phys.* **9**, 3. [DOI](#).
- Yashiro, S., Michalek, G., Gopalswamy, N.: 2008, *Ann. Geophys.* **26**, 3103. [ADS](#). [DOI](#).
- Youssef, M.: 2012, *NRIAG J. Astron. Geophys.* **1**, 172. [ADS](#). [DOI](#).
- Zhang, J., Dere, K.P., Howard, R.A., Kundu, M.R., White, S.M.: 2001, *Astrophys. J.* **559**, 452. [ADS](#). [DOI](#).
- Zhou, G., Wang, J., Cao, Z.: 2003, *Astron. Astrophys.* **397**, 1057. [ADS](#). [DOI](#).
- Zolotova, N.V., Ponyavin, D.I.: 2014, *J. Geophys. Res.* **119**, 3281. [ADS](#). [DOI](#).